Enhanced Thermal and Mechanical Properties of Hydrophobic Graphite-embedded Polydimethylsiloxane Composite

Nikhil Sheshkar[1], Gulshan Verma[1], Chandan Pandey[1], Atul Kumar Sharma[1], Ankur Gupta[1, *]
[1]Department of Mechanical Engineering, Indian Institute of Technology Jodhpur-342037, Rajasthan, India
*Corresponding Author: ankurgupta@iitj.ac.in

Abstract:

This work reports the facile fabrication of graphite embedded polydimethylsiloxane (PDMS) composites using in-situ polymerization and investigates the impact of graphite fillers on their mechanical and thermal characteristics. The extensive characterization is performed using scanning electron microscopy (SEM), contact angle measurement system, thermogravimetric analysis (TGA), and differential scanning calorimetry (DSC). The mechanical properties of the prepared composites are investigated by compression test which explores the possibility of manipulating the PDMS properties by unswervingly modifying the concentration of conductive graphite filler which improves filler dispersion in the PDMS and increases its interaction with graphite fillers, thereby enhancing the mechanical and thermal characteristics of the manufactured composites. The current study confirms the hydrophobicity (contact angle ~112°) of the fabricated composites and investigates the impact of graphite concentrations ranging from 2.5%–20% on the mechanical properties of pure PDMS polymer during compression testing. Furthermore, the thermal conductivity, thermal diffusivity, and specific heat of graphite-embedded PDMS were around 82%, 505% and 1040% higher than that of the pure PDMS, respectively, while the mechanical properties for the compressive module ranged from 3.2 MPa to 4.9 MPa with the elastic behavior up to 40% strain.

Keywords: Polydimethylsiloxane, in-situ polymerization, elastomers

1 Introduction

The rapid progress in the field of miniaturization and integration of portable devices, such as micro/nano-generators [1], micro/nano-actuators, flexible sensors [2], microfluidics devices [3], [4] etc., leads to increase in the heat dissipation issues [5], [6]. Polymer materials have the ability to be used in such fields because of their outstanding versatility and ease of fabrication along with the excellent overall efficiency, good biocompatibility, inertness to various chemicals, thermal stability, adhesion capacity towards other materials. However, due to their low intrinsic electrical and thermal conduction efficiency, they are not suitable for use in high power-density devices [7]. Silicon-based devices were widely preferred due to their small size, high stability and sensitivity, outstanding signal/noise ratio, limited hysteresis and ability to work in dynamic conditions [8]. These devices have been used in a variety of applications including biomedical sciences [9], [10], automotive [11], [12], and environmental field [13]. Some disadvantages included high fabrication costs due to the need for cleanroom infrastructure, high brittleness, which limited their spectrum of assessment in biomedical applications, and saturation in their responses over time. Polymer-based nanocomposites have acknowledged considerable attention in the last two decades due to their importance in the current manufacturing technology.

Soft elastomeric silicone such as Poly-dimethyl siloxane (PDMS), has shown advantages in variety of applications, including structural engineering, wearable and flexible electronics, biomedical and tissue engineering, and many more, due to resistance to climate changes, bio-compatibility, liquidity nature, and dielectric properties [14], [15]. As a result of its low modulus of elasticity and high stretchability, PDMS can be an excellent substrate material used in the fabrication of flexible devices [16], [17]. Pure PDMS has poor mechanical properties and low tear resistance, therefore severely limiting its practical application. Many approaches have been used in the past to improve the thermal stability and electrical conductivity of polymers, which includes the incorporation of various active particles, the addition of certain fillers and the formation of inter-penetrating structures [18].

The conductive network in the matrix defines the conduction property of polymer composites [19], [20]. Further, zero-dimensional (0-D) particles such as metal [21], carbon particles [22],[23] etc. have been widely used to enhance the polymers conductivities, however the increase in conductivity is generally modest due to their low aspect ratio. In this case, constructing a conductive network with low filler loading is difficult to achieve [24]. Increased filler loading improves polymer conductivities but degrades composite processing and mechanical characteristics. One dimensional (1-D) particles, such as carbon nanotube (CNT), are appealing due to the presence of high aspect ratio structures in contrast to 0-D conductive particles [25]. Though, the high aspect ratio causes the diffusion challenging in the polymer matrix. Furthermore, high thermal and electrical resistance limits the improvement of conductivity of the composites beyond the percolation threshold [26]. On comparing the 0-D and 1-D particles, two dimensional (2-D) particles [27], such as graphene are highly appealing as these particles overcome the limitation possessed by the 0-D and 1-D conductive particles [28]. These conductive fillers also upsurge the performance of polymer composites, which could be useful in the areas of energy production and stretchable electronics [29]. Mohamed et al. [30] explored the various ways for inserting Polybenzoxazine/polyhedral oligomeric silsesquioxane (POSS) nanoparticles into poly-imide matrices, including covalent physical blending and chemical bonding. Huang et al. [31] created dual-functionalized cellulose nanofiber via surface-initiated atom transfer radical polymerization (ATRP) and tetramethylpiperidine-1-oxyl (TEMP)-mediated oxidation. Battegazzore et al. prepared a flexible nanocomposite sheet via impregnating PDMS in the porous graphite nano-plates. The fabrication of PDMS/GNP nanosheets tends to be an efficient technique which finds its application in the modern flexible electronics due to its versatility [32]. Sliva et al. described the fabrication of PDMS/graphite composites using additive manufacturing to regenerate a 3D structure for a number of tissues in biomedical applications, such as bone, cartilage [33], cellulose nanofibers [34], [35]. The presence of other nanostructured materials in the PDMS-based composites such as TiO_2, ZrO_2 and Al_2O_3 can enhance heat resistance, thermal conductance, resistance to abrasion and many more [36], [37]. Therefore, it expands the application of PDMS-based composites in various fields. Because of their tiny size and resulting increase in surface area, nanofillers have been widely employed in elastomeric based composites, enabling major improvements in polymer matrix properties at modest filler loadings. The orientation, dispersions, aspect ratio, and size of nanofillers, as well as the interaction mechanisms of fillers, are all elements that influence the reinforcing capability of composites.

In the present study, PDMS/graphite composites using a simple physical blending technique known as in-situ polymerization have been reported. To the best of the authors' knowledge, the mechanical characterization of PDMS and hydrophobic graphite-embedded composite has not hitherto been reported in the literature. The impact of graphite material on the mechanical/thermal characteristics and physical structure of PDMS-based composites has been explored. The manipulation of the material properties of PDMS/graphite composites by directly modifying the concentration of conductive graphite nanofiller, improves filler dispersion in the PDMS and increases the interaction of graphite

nanofillers with PDMS. It enhances the various characteristics viz., of the manufactured composites. The mechanical strength of such composites is a function of the structural characteristics of the fillers. The remainder of the paper is divided into four parts. Section 2 discusses the various materials and procedures for preparing PDMS/graphite composites with different graphite filler concentrations. The experimental characterization information is presented in section 3 and the results are discussed in section 4.

2 Material and method

In this section, we present information on the various materials and methods used for the preparation of PDMS/Graphite composites by varying the concentration of graphite nanofillers. Figure 1 shows the chemical structures of graphite and PDMS. The mechanical properties of the PDMS and PDMS/graphite are examined by manufacturing composite mold. These molds were prepared according to the ASTM standard for tensile and compressive testing. The composite is prepared from the two-part kit containing a Sylgard 184 silicone elastomer base (monomer) and curing agent (cross-linker), which was procured from (Dow Europe GMBH CIO DOW SILICONES, GERMANY) and 20 μm graphite particles with 99.5% purity, were used to fabricate all test specimens. Compression test specimens are made in accordance with ASTM D575-91 specifications. The Avery Denison T42U was used for the compression test. For specific heat tests, a type K thermocouple was used.

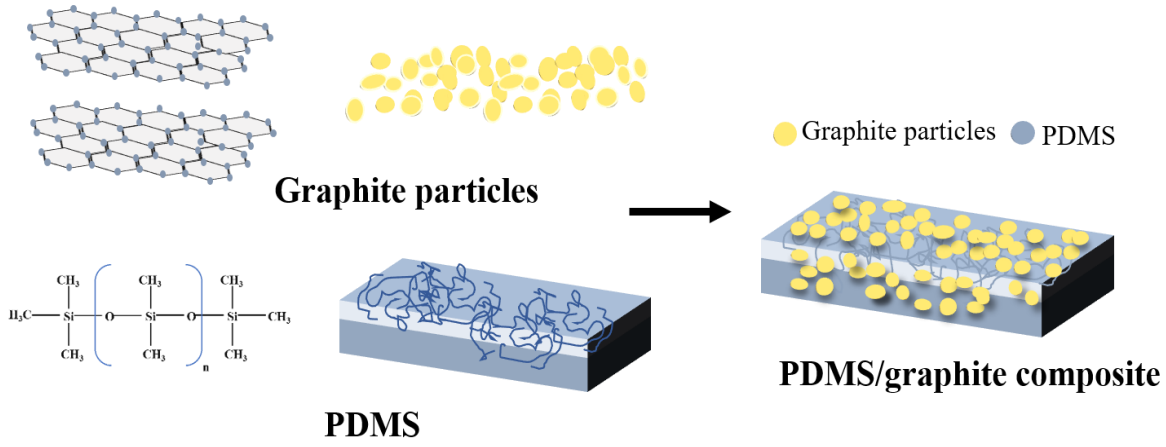

Figure 1. Structural information of PDMS/graphite composite.

2.1 Designing and printing of 3D mold

The dumbbell-shaped tensile test specimens were manufactured as per the American Society for Testing of Materials (ASTM) D412 Type C Standards, where these dumbbell-shaped end segments are fixed to the Universal testing machine, and the narrowed central neck part of the specimen was examined. For performing the compressive testing, the test specimens were manufactured according to the ASTM D575-91 standard. The design of the mold for both tensile and compressive tests is prepared using an additive manufacturing technique which is shown in supplementary information as figure S1.

2.2 Samples preparation of composite

Sylgard 184 silicone elastomer base (monomer) and curing agent (cross-linker) were blended in a 10:1 weight ratio to prepare a Si matrix for the composite. Ultrasonicator was used to shear mix the cross-

linker and monomer for 10 minutes, followed by degassing for 25 minutes and loading the sample in a desiccator to remove trapped air bubbles. Following that, the degasified mixture was transferred to a 3D-printed mold. It was then allowed to cure at 65˚C for 3 hours. The cured sample was then removed from the mold. The same procedure was used to prepare the PDMS/graphite composite sample by incorporating graphite nanofillers into the PDMS. Figure 2 illustrates the comprehensive steps involved in the fabrication of PDMS/graphite composite.

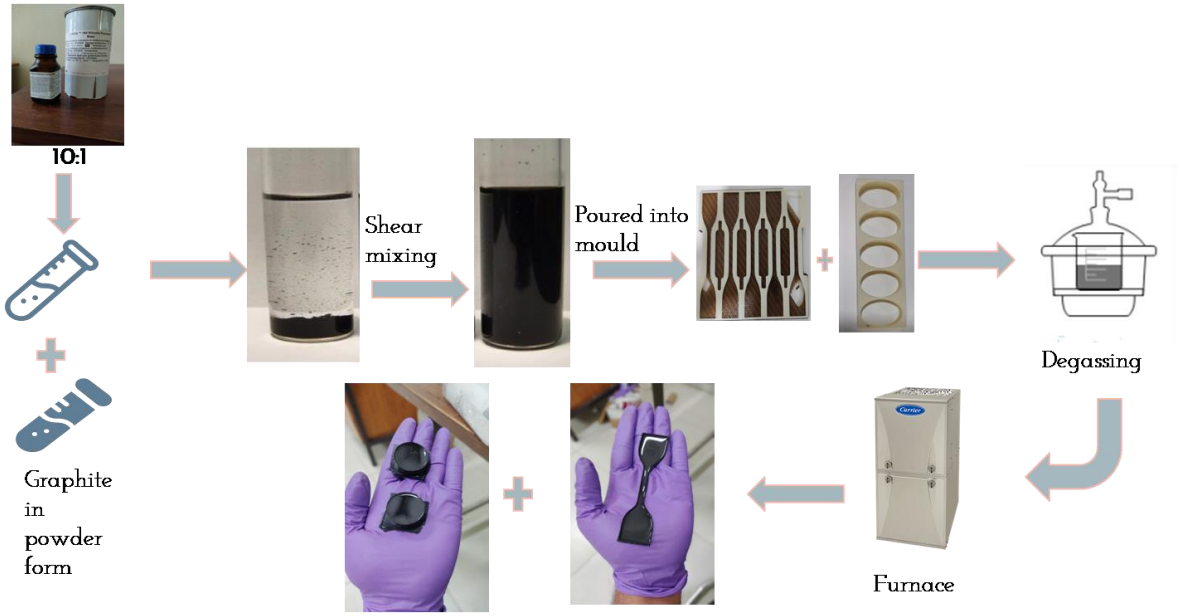

Figure 2 represents the procedure used for the preparation of PDMS-Graphite composite (tensile and compressive test specimens).

3 Experimental characterization

In this section, pure PDMS and PDMS/graphite composites samples were continuously monitored throughout the fabrication process based on their transparency to identify tears, bubbles, and other defects that can affect the mechanical properties. All the samples which are subjected to the mechanical testing are carefully checked for the presence of any deformities so as to ensure proper uniformity in the test results.

3.1 Compressive Test

The compressive strength testing of the pure PDMS and PDMS/Graphite composites were conducted in accordance with the ASTM D-1229-03 standard on a universal testing machine (Company: Ametek Llyod Load capacity-45 kN as shown in figure S2 in supplementary information). The crosshead moved at a rate of 20mm/min. The data was collected under a maximum of 45 kN load conditions during the process. The specimen thickness was reduced from 12mm to 3mm and was tested at room temperature.

3.2 Thermal properties

To investigate the thermal properties of pure PDMS and PDMS/graphite composites, five samples with a diameter of 28mm and a thickness of 12mm were made by varying the concentration of graphite in the composite. The thermal diffusivities (α), thermal conductivity (λ), and specific heat (Cp) of all samples were measured by Thermal Conductivity Analyzers (Hot Disk, Sweden) as shown in figure S3

in supplementary information. The thermal conductivities (λ) of the sample can be verified by using a formula; λ=α ×ρ ×Cp. All specimens were subjected to thermo gravimetric analysis (TGA) using TA Q500 Instruments, which were heated from ambient temperature to 800 °C at a rate of 10 ˚C/ min in a N_2 atmosphere.

3.3 Surface free energy and contact angle measurement

Numerous efforts have been made to analyse and modify the surface properties of PDMS, limiting its applicability in analytical devices. Herein the surface free energy and contact angle measurement have been performed with the help of instrument (Kruss DSA25B).

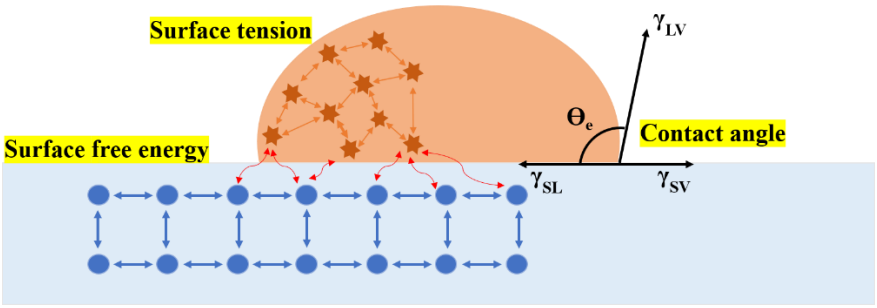

Figure 3. Schematic representation of the sessile drop method.

Contact angle has been measured via sessile drop method, schematic representation of which is shown in figure 3. Herein, when the probe liquid fall on the surface of the solid sample, molecules present at the interface of gas-liquid and liquid-solid surfaces undergoes a strong cohesive forces and weak adhesive forces with their neighboring liquid and gas-solid molecules. This result in surface tension. The similar thing happens at the solid-gas interface. The surface tensions of each of these three surfaces are different: solid-gas γ_{sv}, solid-liquid $\gamma_{sl}$and liquid-gas γ_{lv}. In the three-phase contact line where the solid-liquid-gas meet, each of these surface tensions is balanced by the contact angle (θ_e) formed between the drop and the surface of the solid sample. The wetting phenomenon on the macro scale can be explained by Young's equation.

$$\gamma_{lv} cos\theta e = \gamma_{sv} - \gamma_{sl} \quad (1)$$

Where, γ_{sl} is the energy of solid-liquid interface, γ_{sv} is the energy of the solid surface, γ_{lv} is the surface tension of liquid-vapor interface, and θ is the contact angle. A 0° contact angle represent the wetting conditions while contact angle of 180° represent the non-wetting condition. A hydrophilic surface is one that has a contact angle (< 90°), while a hydrophobic surface has a contact angle (>90°).

The OWRK technique develops a two-component model that separates interfacial tensions based on fundamental interactions between molecules. Polar and dispersive interactions are the terms used to describe these interactions. The total surface energy of a solid is the sum of its two parts. Polar interactions occur by permanent dipole-permanent-dipole interactions. They are strong and exist only in polarity. The dispersive component, is weak and results from random fluctuations in the electron density of the electron cloud, thus inducing temporary dipole interactions. Since in the OWRK method there are two unknowns (solid surface free energy and solid-liquid interface free energy), calculating the solid surface free energy requires at least two liquids for which the dispersed and polar parts of the surface tension are known. The proposed OWRK model are as follows.

$$\gamma_{sl} = \gamma_{sv} + \gamma_{lv} - 2\left(\sqrt{\gamma_{sv}^{P}\gamma_{lv}^{P}} + \sqrt{\gamma_{sv}^{D}\gamma_{lv}^{D}}\right) \quad (2)$$

Where, γ_{sv}^{P} and γ_{lv}^{P} are polar components and γ_{sv}^{D} and γ_{lv}^{D} are dispersive components of solid surface energy and liquid surface energy, respectively.

Replacing the value of γ_{sl} from eq (1).

$$\sqrt{\gamma_{sv}^{P}\gamma_{lv}^{P}} + \sqrt{\gamma_{sv}^{D}\gamma_{lv}^{D}} = \frac{[\gamma_{sv}+\gamma_{lv}-(\gamma_{sv}-\gamma_{lv}\cos\theta e)]}{2} \quad (3)$$

$$\sqrt{\gamma_{sv}^{P}\gamma_{lv}^{P}} + \sqrt{\gamma_{sv}^{D}\gamma_{lv}^{D}} = \frac{[\gamma_{sv}(1+\cos\theta e)]}{2} \quad (4)$$

The above-mentioned equations are helpful in estimating the surface free energy of the composite films.

4 Result and discussion

4.1 Structural Characterization

Scanning electron microscope **(**SEM-Carl Zeiss, EDS-Oxford instruments**)** was used to study the surface morphology of all samples as well as the micro-distribution of the nanoparticles in the composites. The images were obtained at magnifications of 300X to 500X at an accelerating voltage of 20 kV. The analysis describes the distribution of particles and intermolecular bonding on the composite and the filler material which is responsible for the irregular surface. Figure 4 depicts the SEM views of PDMS/graphite composite that reveals the surface morphologies.

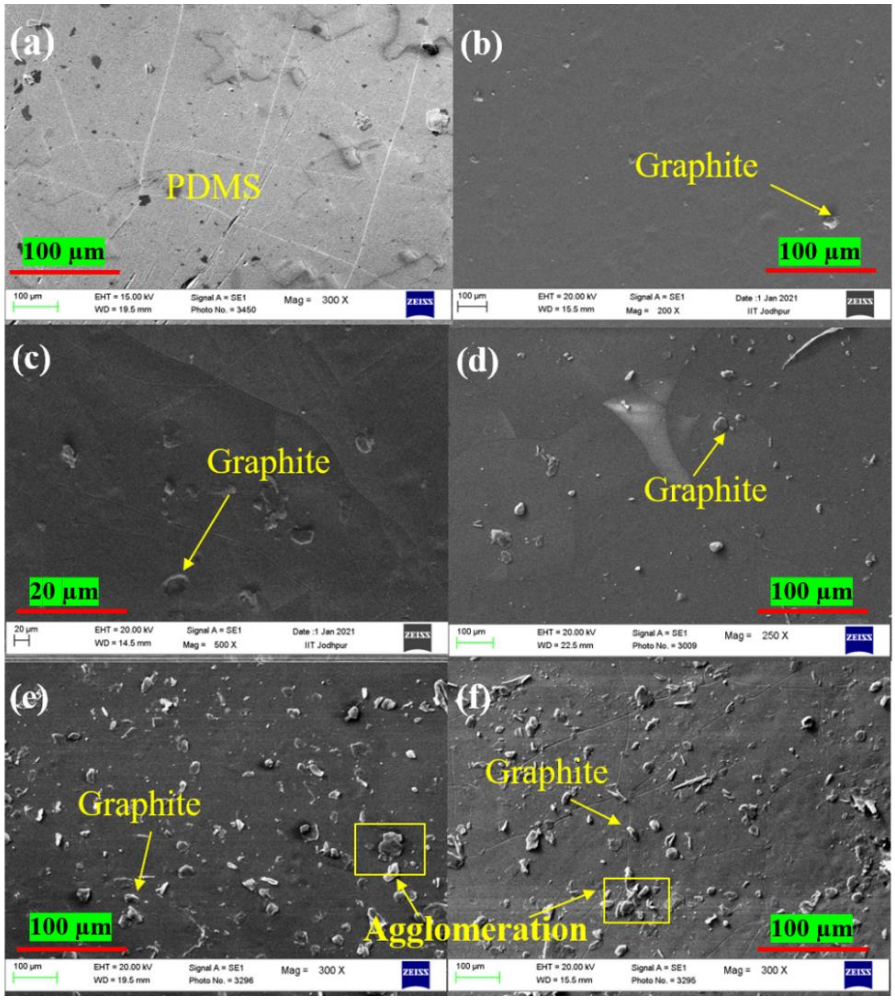

Figure 4. Scanning electron microscope images of (a) pure PDMS, (b) 2.5%, (c) 5%, (d) 10%, (e) 15%, (f) 20 wt% PDMS/graphite composite.

The structural properties of nanofillers, as well as the qualities of the composite material as a whole, are heavily influenced by its structural qualities. As the reinforcing concentration is raised, the filler material produces either huge irregular or small aggregates. Such aggregates are created during the preparation process. The fractured surfaces of pure PDMS and PDMS/graphite composites were analyzed using SEM. The SEM image of the pure PDMS and PDMS after graphite addition is shown in Fig. 4. A uniform distribution of the graphite particles with less density is observed for graphite concentration up to 10% (Fig. 3b-d). However, an increase in graphite concentration beyond 10% leads to the agglomeration of the graphite particles, which also might be the cause of a reduction in mechanical properties. From Fig. 4, various SEM results are observed, such as the modes of fractures, interfacial bond in the composite sample, and the distribution of the particles. Graphite particles inside the matrix are marked clearly. The compressive strength of the composites improved as the proportion of filler in the matrix increased until 15 % reinforcement was achieved, indicating an increase in graphite content in PDMS. Furthermore, the higher compressive strength attained with 15% graphite superiority could be attributed to effective interfacial bonding between graphite and the PDMS, as illustrated in Figure 4 (e), in contrast to a larger filler content. Following that, bonding and particle dispersion become less uniform, potentially lowering the strength of the composite. Figures 4 (e) and 3 (f) depict improper bonding of higher percentage composites. Additionally, agglomeration of the filler particles may occur as a result of additional reinforcement, resulting in a loss in mechanical characteristics.

4.2 Compression Test

Compression tests were performed on six different samples, including 2.5%, 5%, 10%, 15% and 20 wt % graphite nanofillers in PDMS and pure PDMS. Up to 40% strain, all six curves are linear, but after that, they become nonlinear. Figure 5(a) displays the stress–strain relation of PDMS and PDMS/graphite composite at 2.5–20 wt %. At 9 mm compression, 15 wt% PDMS/graphite can bear the highest compressive load, followed by PDMS/graphite composites of 10 wt% and 5 wt%. Figure 4(b) depicts the result of compressive modulus. The compressive test results of pure PDMS and PDMS/graphite composite at 40% strain are shown in Table 1.

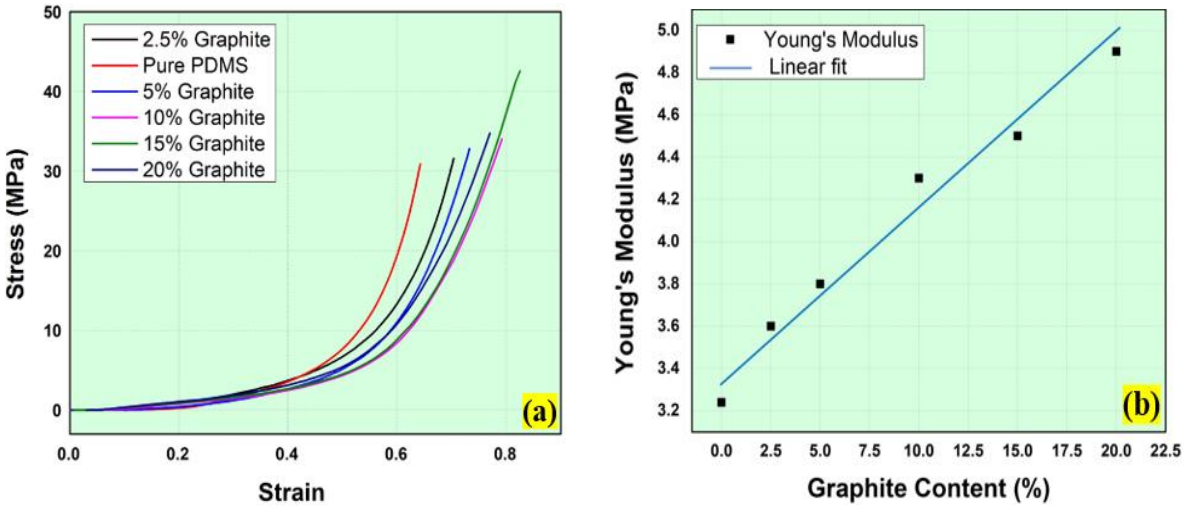

Figure 5. Relation between (a) stress-strain curve, and (b) compressive modulus.

Table 1. Compressive test results of pure PDMS and PDMS/graphite composite at 40% strain.

Filler content in PDMS	Stress (MPa)	Strain	Young's Modulus (MPa)
Pure PDMS	30.882	0.40046	3.2
2.5% PDMS/Graphite	31.591	0.40052	3.6
5% PDMS/Graphite	32.812	0.40158	3.8
10% PDMS/Graphite	33.983	0.40364	4.3
15% PDMS/Graphite	42.557	0.40374	4.5
20% PDMS/Graphite	34.740	0.40038	4.9

4.3 Thermal Properties

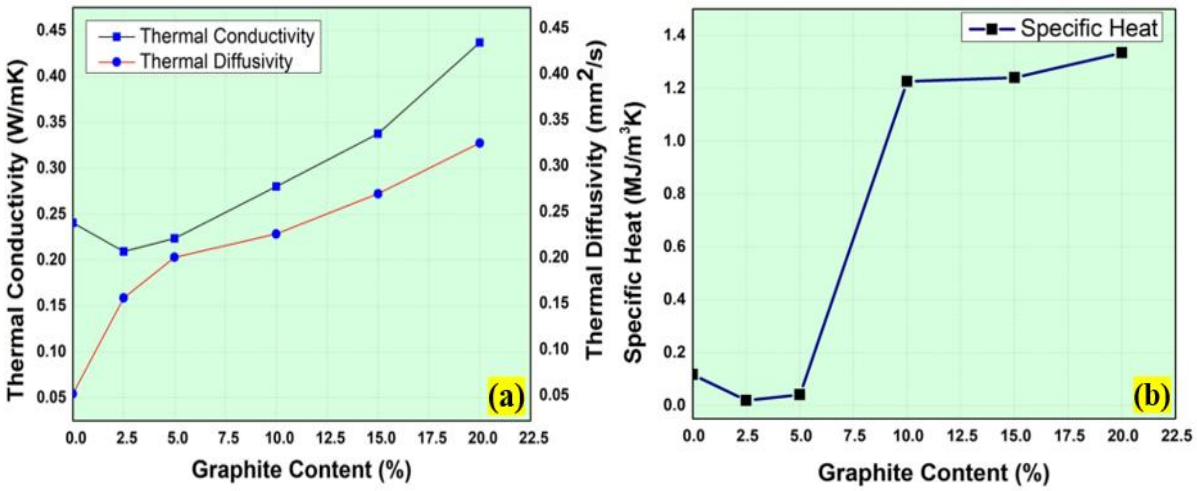

Figure 6. (a) Thermal conductivity and thermal diffusivity of composite, (b) Specific heat change in samples with varying graphite concentration.

For investigating the effect of graphene, the thermal conductivity of PDMS/graphite composites with varying concentrations of graphite under various conditions was investigated. Figure 6(a), shows that with the increase of graphite nanofillers into the polymer matrix, the thermal conductivity of the PDMS/graphite composites increases. Pure PDMS has a thermal conductivity of 0.2405 W/mK, which is insufficient to satisfy the thermal management challenges of various contemporary electronic devices. In comparison to the pure PDMS, the thermal conductivity of PDMS/graphite composite samples having 2.5%, 5%, 10%, 15% and 20% graphite by weight was enhanced to 0.2094, 0.2235, 0.2801, 0.3376 and 0.4370 W/mK, respectively. The sample with 20 wt% graphite nanofiller in the PDMS/graphite composite shows an 81.7 % enhancement of thermal conductivity w.r.t pure PDMS. The results of the thermal characteristics of pure PDMS and PDMS/graphite composite are shown in Table 2. The reason for the improvement of thermal conductivity is the formation of a graphite nanofiller network inside the polymer matrix. Moreover, the creation of a small thermal interface and the high aspect ratio aided the formation of a cross-linked graphite interconnect network with higher thermal transport efficiency.

Table 2. Thermal properties of pure PDMS and PDMS/graphite composite.

Filler content in PDMS	Thermal Conductivity (W/mK)	Thermal Diffusivity (mm^2/s)	Specific Heat (MJ/m^3K)

Pure PDMS	0.240	0.054	0.117
2.5% PDMS/Graphite	0.209	0.159	0.019
5% PDMS/Graphite	0.224	0.203	0.041
10% PDMS/Graphite	0.280	0.228	1.226
15% PDMS/Graphite	0.338	0.272	1.241
20% PDMS/Graphite	0.437	0.327	1.334

4.4 DSC and TGA measurements

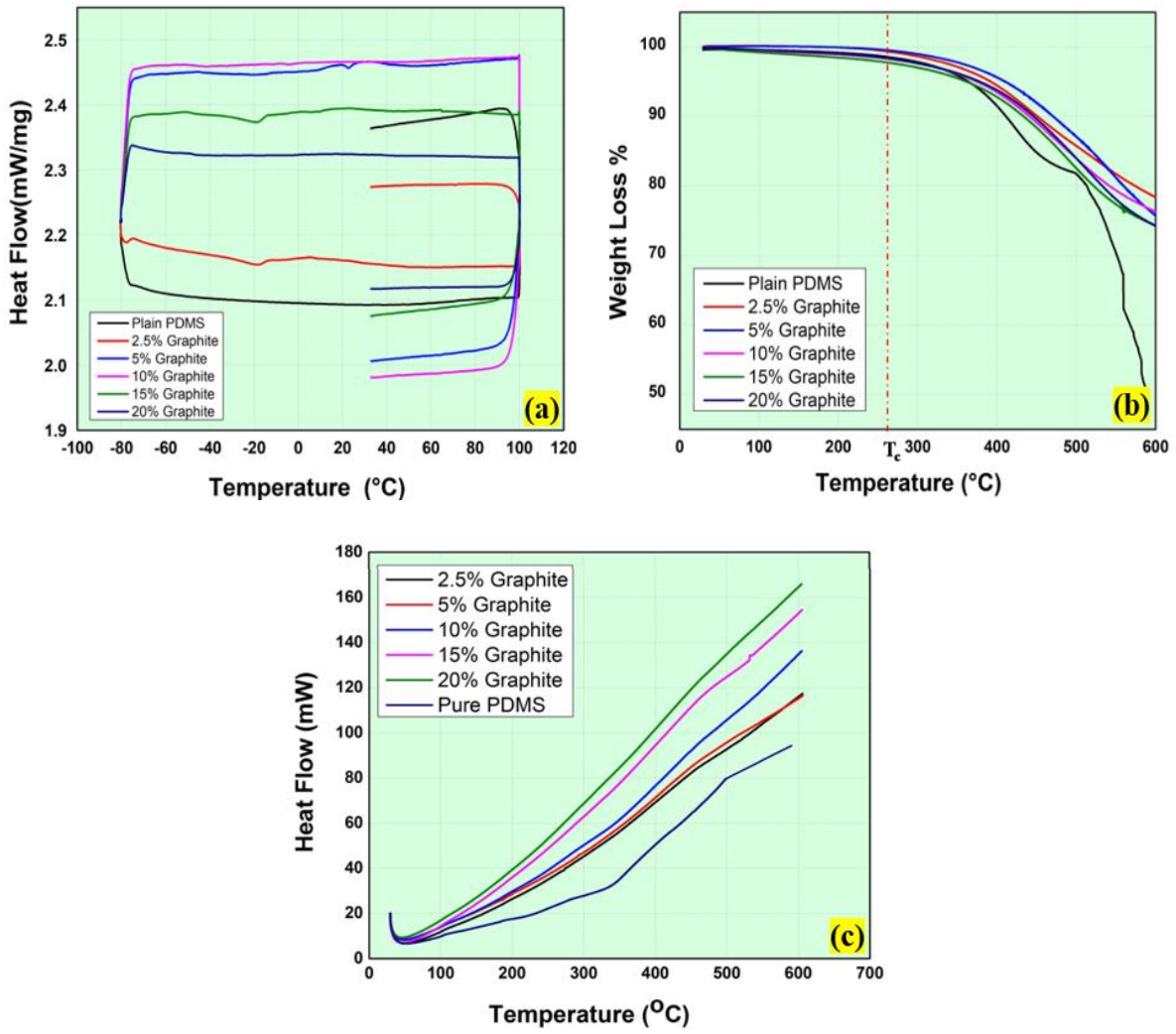

Figure 7 (a) DSC, (b) and (c) TGA results for pure and PDMS/graphite composites.

Except in the case of extremely low molecular weights of polymer, PDMS is a semi-crystalline polymer with a high crystallinity, based on cooling conditions. The filler has a considerable impact on crystallization in PDMS based composites. The effects of the nanofillers on the thermal characteristics of Polydimethylsiloxane, particularly crystallization and glass transition, are the main focus of this study. According to earlier research, both the existence of a nanofiller and crystallization can influence the strength and temperature in semicrystalline polymers [38]. In DSC, generally three measurement routes are followed, such as (i) rapid cooling, (ii) standard cooling, (iii) isothermal crystallization heating. We employed the standard cooling procedure to determine the thermal properties associated with the PDMS based composites. The prepared PDMS based sample is cooled to -80˚C at a constant rate of 10 K/min and then heated up to a temperature of 100˚C at 10 K/min, again cooled to 30˚C i.e.,

melt state associated with PDMS. From figure 7, between pure and different filler fractions of PDMS/graphite composite, DSC tests revealed no significant glass transition temperature because of the instrument operating temperature constraint. The heat flow of 2.5%, 5%, 10%, 15% and 20% of PDMS/graphite composites is around 2.761%, 18.334 %, 18.232 %, 14.438% and 11.715% greater than the pure PDMS sample respectively.

Figure 7 depicts that the heat flow in the PDMS/graphite composite is greater than that in pure PDMS. Fourier's law of heat has a direct relationship between heat flow and thermal resistance i.e., $Q= \Delta T/R$ [39]. At a certain temperature ramp, "Q" is defined as the rate of heat flow for a PDMS sample w.r.t rate of heat flow of reference sample. "R" is defined as the thermal resistance and "ΔT" is the difference of temperature between the sample-reference. As a result, the lower the effective thermal resistance, the higher the heat flow. Furthermore, no phase change, such as crystallization, has been observed, indicating that the graphite nanofillers are very well accommodated inside the PDMS.

The decomposition losses of pure PDMS and PDMS/graphite composites occurred primarily at ~ 500 °C as shown in the figure 7(b). Figure 6(c), depicts the relation between the heat flow and temperature. In all cases, the 1% weight loss (T_c) was obtained around 265 °C. Decomposition of the pure PDMS proceeded in two steps, indicating that there is a chemical-based transition that might be related to depolymerization of the material. However, similar processes are not observed in any PDMS/graphite composites, implying that the substance undergoes immediate decomposition. This finding suggests that graphite nanofiller were used to cross-link the pure PDMS polymer chains.

4.5 Contact angle measurement results

Figure 8 shows the water droplet profile over fabricated substrates. Further using the Kruss advance software, the contact angles were used to measure the surface free energy (SFE) of the PDMS and PDMS/Graphite composite using the OWRK method. A contact angle (< 90˚) indicates that surface wetting is beneficial, and the liquid will spread to a large area of the surface; whereas a contact angle (>90˚) usually indicates that surface wetting is unfavorable, and the liquid will reduce contact with the surface and produce a droplet. The conventional meaning of contact angle is the angle made by a liquid when it is deposited on a solid or liquid. Smaller contact angles result in weaker cohesion than adhesion, and the interaction of liquid molecules with solid molecules is frequently greater than the interaction with liquid molecules. More a contact angle, stronger the cohesion, and the interaction between the molecules in the liquid is often greater with each other than with the solid molecules. The results demonstrate that the cohesion is greatly improved compared to adhesion with the enhanced contact angle of the PDMS/graphite composite in contrast to pure PDMS. Table 3 and 4 shows the values of surface tension and surface free energy.

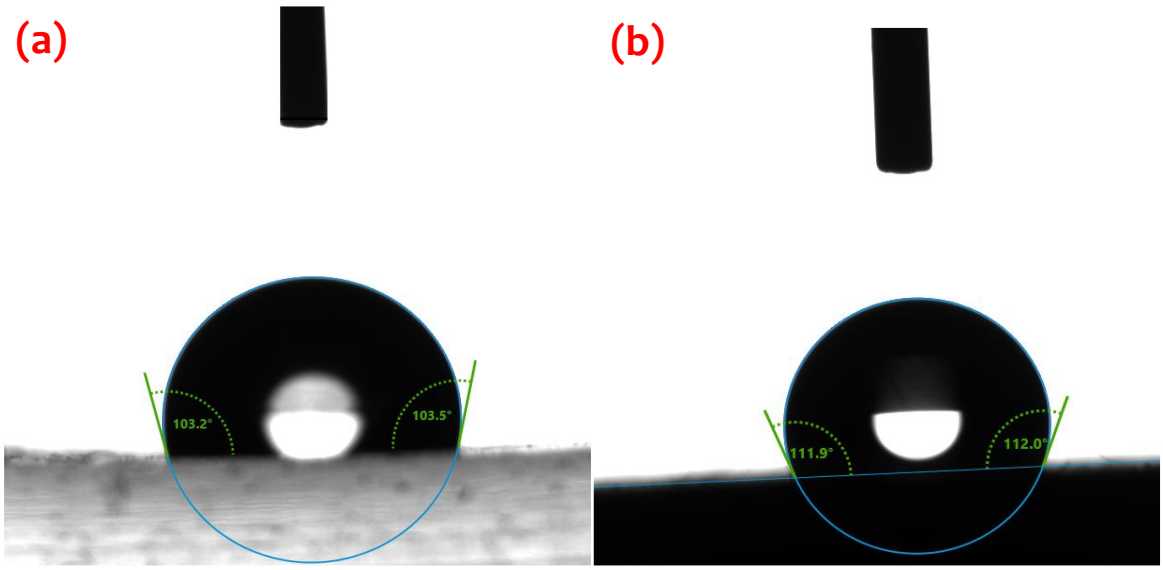

Figure 8. Representation of the sensile drop (water) with measured angles (a) PDMS (CA: 103.5˚), (b) PDMS/graphite composites (CA: 112.0˚).

Table 3. The surface tension component of the liquid used to measure the surface free energy (SFE) at 25 ° C.

Probe Liquid	SFT	Polar	Disperse
Toluene	28.4 mN/m	2.3 mN/m	26.1 mN/m
Water	72.8 mN/m	51 mN/m	21.8 mN/m

Table 4. Surface free energy and contact angle results for PDMS and PDMS/graphite composite**.**

Materials	Contact angle	SFE total (mN/m)	SFE disperse (mN/m)
PDMS	103.5	23.08 ± 0.42	22.95 ± 0.34
PDMS/graphite	112.0	27.01 ± 0.84	27.07 ± 0.83

5 Conclusion

In the current study, the mechanical properties of hydrophobic graphite reinforced PDMS composite material were evaluated. The effects of graphite on simple PDMS polymers were studied at concentrations ranging from 2.5% – 20%. These experiments yielded mechanical characteristics such as compressive modulus, thermal diffusivity, conductivity, and specific heat. The thermal conductivity, thermal diffusivity and specific heat of graphite-filled PDMS was around 82%, 505% and 1040% respectively higher than that of the pure PDMS, while mechanical properties for compressive module as 3.2 MPa to 4.9 MPa with the elastic behavior up to 40% strain. The compressive modulus of the 20% graphite-filled material was around 42% higher than that of the pure PDMS, and varied linearly with the increased graphite content percentage filler. Current study on graphite inclusion in simple PDMS provides succinct data for designing sensors and actuators, photothermal and electrothermal based actuators, and electronic systems. Furthermore, the testing and manufacture of compressive approaches for pure PDMS and PDMS/graphite composite samples may aid in the advancement of future structural systems. The findings reported in this work will be helpful in the design and development of composite-based prosthetics, diaphragms and pressure sensors.

Acknowledgements

Corresponding author would like to acknowledge the affiliating institute (IIT Jodhpur) to provide the research seed grant (I/SEED/AKG/20190022) which was helpful in accomplishing the reported work.

Conflicts of Interest

The authors declare no conflict of interest. The funders had no role in the design of the study; in the collection, analyses, or interpretation of data; in the writing of the manuscript, or in the decision to publish the results.

References

[1] S. Nambiar and J. T. W. Yeow, "Conductive polymer-based sensors for biomedical applications," *Biosens. Bioelectron.*, vol. 26, no. 5, pp. 1825–1832, 2011, doi: 10.1016/j.bios.2010.09.046.

[2] A. Gupta and P. Pal, "Flexible Sensors for Biomedical Application," in *Environmental, Chemical and Medical Sensors*, 2018, pp. 287–314.

[3] A. Atwe, A. Gupta, R. Kant, M. Das, I. Sharma, and S. Bhattacharya, "A novel microfluidic switch for pH control using Chitosan based hydrogels," *Microsyst. Technol.*, vol. 20, no. 7, pp. 1373–1381, 2014, doi: 10.1007/s00542-014-2112-0.

[4] R. K. Singh, R. Kant, S. Singh, E. Suresh, A. Gupta, and S. Bhattacharya, "A novel helical micro-valve for embedded micro-fluidic applications," *Microfluid. Nanofluidics*, vol. 19, no. 1, pp. 19–29, 2015, doi: 10.1007/s10404-015-1543-y.

[5] X. Xu, J. Chen, J. Zhou, and B. Li, "Thermal Conductivity of Polymers and Their Nanocomposites," *Adv. Mater.*, vol. 30, no. 17, pp. 1–10, 2018, doi: 10.1002/adma.201705544.

[6] J. Wang *et al.*, "Flexible and wearable PDMS-based triboelectric nanogenerator for self-powered tactile sensing," *Nanomaterials*, vol. 9, no. 9, 2019, doi: 10.3390/nano9091304.

[7] L. Xie and Y. Zhu, "Tune the Phase Morphology to Design Conductive Polymer Composites: A Review," *Polym. Polym. Compos.*, vol. 16, no. 2, pp. 101–113, 2008, doi: 10.1002/pc.

[8] Y. Xu, X. Hu, S. Kundu, A. Nag, N. Afsarimanesh, and S. Sapra, "Silicon-Based Sensors for Biomedical Applications: A Review," *sensors*, vol. 19, pp. 1–22, 2019, doi: doi:10.3390/s19132908.

[9] R. K. Singh, A. Kumar, R. Kant, A. Gupta, E. Suresh, and S. Bhattacharya, "Design and fabrication of 3-dimensional helical structures in polydimethylsiloxane for flow control applications," *Microsyst. Technol.*, vol. 20, no. 1, pp. 101–111, 2014, doi: 10.1007/s00542-013-1738-7.

[10] M. Nayak *et al.*, "Integrated sorting, concentration and real time PCR based detection system for sensitive detection of microorganisms," *Sci. Rep.*, vol. 3, pp. 1–7, 2013, doi: 10.1038/srep03266.

[11] G. Kumar Verma and M. Z. Ansari, "Design and simulation of piezoresistive polymer accelerometer," *IOP Conf. Ser. Mater. Sci. Eng.*, vol. 561, no. 1, 2019, doi: 10.1088/1757-

899X/561/1/012128.

[12] A. K. Naskar, J. K. Keum, and R. G. Boeman, “Polymer matrix nanocomposites for automotive structural components,” *Nat. Nanotechnol.*, vol. 11, no. 12, pp. 1026–1030, 2016, doi: 10.1038/nnano.2016.262.

[13] J. H. Koo, *Fundamentals, properties, and applications of polymer nanocomposites*. 2016.

[14] Sharma, A., Pandey, A., Shukla, D. K., & Pandey, K. N. (2018). Effect of self-healing dicyclopentadiene microcapsules on fracture toughness of epoxy. Materials Today: Proceedings, 5(10), 21256-21262.

[15] A. Camenzind, T. Schweizer, M. Sztucki, and S. E. Pratsinis, “Structure & strength of silica-PDMS nanocomposites,” *Polymer (Guildf).*, vol. 51, no. 8, pp. 1796–1804, 2010, doi: 10.1016/j.polymer.2010.02.030.

[16] A. K. Sharma, N. Sheshkar, and A. Gupta, “Static and dynamic stability of dielectric elastomer fiber composites,” *Mater. Today Proc.*, vol. 44, no. January, pp. 2043–2047, 2021, doi: 10.1016/j.matpr.2020.12.151.

[17] A. Nag, S. C. Mukhopadhyay, and J. Kosel, “Wearable Flexible Sensors: A Review,” *IEEE Sens. J.*, vol. 17, no. 13, pp. 3949–3960, 2017, doi: 10.1109/JSEN.2017.2705700.

[18] C. Chen, X. Bu, Q. Feng, and D. Li, “Cellulose nanofiber/carbon nanotube conductive nano-network as a reinforcement template for polydimethylsiloxane nanocomposite,” *Polymers (Basel).*, vol. 10, no. 9, pp. 4–13, 2018, doi: 10.3390/polym10091000.

[19] M. G. Mohamed and S. W. Kuo, “Functional Silica and Carbon Nanocomposites Based on Polybenzoxazines,” *Macromol. Chem. Phys.*, vol. 220, no. 1, pp. 1–13, 2019, doi: 10.1002/macp.201800306.

[20] M. G. Mohamed *et al.*, “Multifunctional polyhedral oligomeric silsesquioxane (POSS) based hybrid porous materials for CO2 uptake and iodine adsoprtion,” *Polymers (Basel).*, vol. 13, no. 2, pp. 1–15, 2021, doi: 10.3390/polym13020221.

[21] M. G. Mohamed, N. Y. Liu, A. A. F. EL-Mahdy, and S. W. Kuo, “Ultrastable luminescent hybrid microporous polymers based on polyhedral oligomeric silsesquioxane for CO2 uptake and metal ion sensing,” *Microporous Mesoporous Mater.*, vol. 311, p. 110695, 2021, doi: 10.1016/j.micromeso.2020.110695.

[22] M. G. Mohamed, K. C. Hsu, and S. W. Kuo, “Bifunctional polybenzoxazine nanocomposites containing photo-crosslinkable coumarin units and pyrene units capable of dispersing single-walled carbon nanotubes,” *Polym. Chem.*, vol. 6, no. 13, pp. 2423–2433, 2015, doi: 10.1039/c5py00035a.

[23] M. M. Samy, M. G. Mohamed, and S. W. Kuo, “Pyrene-functionalized tetraphenylethylene polybenzoxazine for dispersing single-walled carbon nanotubes and energy storage,” *Compos. Sci. Technol.*, vol. 199, no. May, p. 108360, 2020, doi: 10.1016/j.compscitech.2020.108360.

[24] M. Karkri, L. Ibos, and B. Garnier, “Comparison of experimental and simulated effective thermal conductivity of polymer matrix filled with metallic spheres: Thermal contact resistance and particle size effect,” *J. Compos. Mater.*, vol. 49, no. 24, pp. 3017–3030, 2015, doi: 10.1177/0021998314559062.

[25] P. Bhawal, S. Ganguly, T. K. Das, S. Mondal, L. Nayak, and N. C. Das, “A comparative study

of physico-mechanical and electrical properties of polymer-carbon nanofiber in wet and melt mixing methods," *Mater. Sci. Eng. B Solid-State Mater. Adv. Technol.*, vol. 245, no. April 2018, pp. 95–106, 2019, doi: 10.1016/j.mseb.2019.05.020.

[26] B. Mensah, K. C. Gupta, H. Kim, W. Wang, K. U. Jeong, and C. Nah, "Graphene-reinforced elastomeric nanocomposites: A review," *Polym. Test.*, vol. 68, no. April, pp. 160–184, 2018, doi: 10.1016/j.polymertesting.2018.04.009.

[27] F. Paquin, J. Rivnay, A. Salleo, N. Stingelin, and C. Silva, "Multi-phase semicrystalline microstructures drive exciton dissociation in neat plastic semiconductors," *J. Mater. Chem. C*, vol. 3, pp. 10715–10722, 2015, doi: 10.1039/b000000x.

[28] A. A. Balandin, "Thermal properties of graphene and nanostructured carbon materials," *Nat. Mater.*, vol. 10, no. 8, pp. 569–581, 2011, doi: 10.1038/nmat3064.

[29] L. Zhao, Y. Yin, B. Jiang, Z. Guo, C. Qu, and Y. Huang, "Fast room-temperature self-healing siloxane elastomer for healable stretchable electronics," *J. Colloid Interface Sci.*, vol. 573, pp. 105–114, 2020, doi: 10.1016/j.jcis.2020.03.125.

[30] M. G. Mohamed and S. W. Kuo, "Functional polyimide/polyhedral oligomeric silsesquioxane nanocomposites," *Polymers (Basel).*, vol. 11, no. 1, 2019, doi: 10.3390/polym11010026.

[31] C. F. Huang, J. K. Chen, T. Y. Tsai, Y. A. Hsieh, and K. Y. Andrew Lin, "Dual-functionalized cellulose nanofibrils prepared through TEMPO-mediated oxidation and surface-initiated ATRP," *Polymer (Guildf).*, vol. 72, pp. 395–405, 2015, doi: 10.1016/j.polymer.2015.02.056.

[32] D. Battegazzore and A. Fina, "Flexible and Highly Conductive Composites By Impregnation of Polydimethylsiloxane in Graphite Nanoplates Paper," pp. 1–10.

[33] M. Silva, I. S. Pinho, J. A. Covas, N. M. Alves, and M. C. Paiva, "3D printing of graphene-based polymeric nanocomposites for biomedical applications," *Funct. Compos. Mater.*, vol. 2, no. 1, 2021, doi: 10.1186/s42252-021-00020-6.

[34] A. L. Goffin *et al.*, "Poly(ε-caprolactone) based nanocomposites reinforced by surface-grafted cellulose nanowhiskers via extrusion processing: Morphology, rheology, and thermo-mechanical properties," *Polymer (Guildf).*, vol. 52, no. 7, pp. 1532–1538, 2011, doi: 10.1016/j.polymer.2011.02.004.

[35] C. W. Tu *et al.*, "Surface-Initiated Initiators for Continuous Activator Regeneration (SI ICAR) ATRP of MMA from 2,2,6,6-tetramethylpiperidine-1-oxy (TEMPO) Oxidized Cellulose Nanofibers for the Preparations of PMMA Nanocomposites," *Polymers (Basel).*, vol. 11, no. 10, 2019, doi: 10.3390/polym11101631.

[36] A. Lamberti, "Microfluidic photocatalytic device exploiting PDMS/TiO 2 nanocomposite," *Appl. Surf. Sci.*, vol. 335, pp. 50–54, 2015, doi: 10.1016/j.apsusc.2015.01.239.

[37] M. Alkahtany, "Color Stability , Physical Properties and Antifungal Effects of ZrO2 and TiO2 Nanoparticle Additions to Pigmented Polydimethylsiloxanes," 2016.

[38] P. Klonos *et al.*, "Morphology, crystallization and rigid amorphous fraction in PDMS adsorbed onto carbon nanotubes and graphite," *Polymer (Guildf).*, vol. 139, pp. 130–144, 2018, doi: 10.1016/j.polymer.2018.02.020.

[39] J.-S. Boisvert *et al.*, "Photosensitised PDMS for femtosecond laser writing," *OSA Contin.*, vol. 3, no. 5, p. 1334, 2020, doi: 10.1364/osac.386533.